Original Research

Differentiation of Prostatic Carcinoma and Benign Prostatic Hyperplasia: Correlation Between Dynamic Gd-DTPA-Enhanced MR Imaging and Histopathology

Lindsay W. Turnbull, FRCR, MD,[1] David L. Buckley, PhD,[1] Lesley S. Turnbull, MRCPath,[2] Gary P. Liney, PhD,[1] and Adrian J. Knowles, DCR[1]

One of the major factors limiting the staging accuracy of conventional magnetic resonance imaging (MRI) for prostatic carcinoma, is the similarity in signal intensity between tumor and coexisting benign prostatic hyperplasia (BPH). As neovascularity is an independent indicator of pathological state, dynamic contrast-enhanced MRI may yield additional information. This study correlates the histopathological findings from 12 radical prostatectomy patients on a region-by-region basis, with pharmacokinetic modeling of dynamic contrast-enhanced (0.2 mmol dimeglumine gadopentetate/kg), fast multiplanar spoilt gradient-recalled echo images, using a two-compartment simplex minimization technique. Quantitative analysis demonstrated differences in the amplitude of the initial contrast upslope and contrast exchange rate between tumor and fibromuscular BPH ($P < 0.03$ and $P < 0.03$, respectively) and for the contrast exchange rate between tumor and fibroglandular BPH ($P < 0.04$), providing improved delineation of intraprostatic tumor extent compared with conventional imaging techniques. J. Magn. reson. Imaging 1999; 9:311–316. © **1999 Wiley-Liss, Inc.**

Index terms: dynamic MR imaging; histopathology; prostate

MAGNETIC RESONANCE IMAGING (MRI) has been used increasingly to image the prostate since the introduction of the endorectal (ER) surface coil and fast spin-echo (FSE) scanning techniques. The use of an ER coil has resulted in overall staging accuracy rates for prostatic tumor of between 68% and 82%, although staging of local disease is considerably poorer at 57% (1–3). The major factors thought to limit the staging accuracy of MRI include the signal intensity of the primary tumor and the resulting determination of intraprostatic tumor location and size. Most tumors are hypointense on T2-weighted sequences and are situated in the peripheral zone, where approximately 70% are readily detected by MRI. However, it is recognized that MRI both over- and underestimates tumor volume. Even with an ER coil, Lencioni et al (4), using T2-weighted FSE images, obtained volume measurements that were only accurate to within 50% of the pathological tumor volume measurement, in 92% of patients examined. This was thought to be due to the similarity in signal intensity between tumor and central gland tissue: poor discrimination resulted, particularly in the presence of coexisting benign disease. This inability to identify the tumor margins accurately may also result in unrecognized proximity to the prostatic capsule, a feature considered an important predictor of transcapsular tumor spread and hence correct local tumor staging.

Dimeglumine gadopentetate (Gd-DTPA)-enhanced MRI with dynamic data acquisition has been shown to improve significantly tissue characterization and assessment of disease extent in other solid tumors (5). Although contrast enhancement is seldom used in prostatic disease, current reports suggest that postcontrast T1-weighted spin-echo (SE) scanning does not improve the accuracy of detection or intraglandular staging of prostate cancer compared with T2-weighted FSE imaging (6,7). The purpose of this study was to examine the ability of dynamic contrast-enhanced MRI, analyzed quantitatively by pharmacokinetic modeling, to differentiate histologically proven benign from malignant prostatic disease to determine the intraprostatic tumor extent.

MATERIALS AND METHODS

Patient Population

Twelve patients with newly diagnosed prostatic adenocarcinoma underwent MRI. They were all candidates for radical prostatectomy on the basis of transrectal ultrasound findings, negative radioisotope bone scan, prostate-specific antigen (PSA) level, and prostate biopsy. The patients ranged from 57 to 70 years of age, with an

[1]Centre for Magnetic Resonance Investigations, Department of Medical Physics, Hull Royal Infirmary, Hull HU2 3JZ, United Kingdom.

[2]Department of Pathology, University of Liverpool, Liverpool L69 3BX, United Kingdom.

Contract grant sponsor: Yorkshire Cancer Research Campaign; contract grant sponsor: Jeremy Drake Foundation.

Presented at the ISMRM Annual Meeting, Nice, 1995.

Address reprint requests to: L.W.T., Centre for Magnetic Resonance Investigations, Hull Royal Infirmary, Anlaby Road, Hull HU3 2JZ, United Kingdom.

Received May 21, 1998; Accepted August 26, 1998.

average age of 65 years. The diagnosis of prostatic neoplasm was made 4–6 weeks prior to MRI by ultrasound-guided transrectal biopsy using a conventional double-line technique to sample left and right aspects of the apex, middle, and base of the gland, with further biopsies of ultrasonically suspicious areas. The mean PSA level was 9.5 ng/mL, ranging from 4.7 to 15.8 ng/mL. The Gleason grade of the biopsy specimens, defined as the sum of the scores of the primary and secondary patterns or twice the score if only a single pattern was detected, ranged from 3 to 5.

Imaging Technique

MRI was performed in the supine position using a 1.5 T superconducting magnet (Signa Advantage, 5.4.2 version software; General Electric, Milwaukee, WI) with an integrated endorectal pelvic phased-array multicoil (Medrad, Pittsburgh, PA). Intravenous buscopan was administered to minimize peristaltic artifact. An initial sagittal localizing scan was obtained to ensure accurate positioning of the ER coil and for positioning of the axial images. Images perpendicular to the posterior aspect of the prostate gland were obtained from the seminal vesicles to the prostatic apex using a heavily T2-weighted FSE sequence (TR 3400 msec, TE 160 msec; ETL 8; echo spacing 17 msec; field of view (FOV) 14 cm; matrix 256 × 192; 4 excitations; 4 mm slice thickness and 1 mm slice gap; 16 kHz bandwidth). Thirty-five sequential images were then acquired dynamically at four preselected slice locations through the prostate, using a fast multiplanar spoilt gradient-recalled echo (FMPSPGR) sequence (TR 10.4 msec, TE 2.9 msec; flip angle 25°; FOV 20 cm; matrix size 256 × 128; 2 excitations; slice thickness 6–7 mm; 2 mm interslice gap). This resulted in a temporal resolution of approximately 11 seconds. Gd-DTPA (Magnevist, Schering, Berlin, Germany) was administered by direct intravenous injection at a dose of 0.2 mmol/kg body weight through an indwelling IV cannula immediately prior to the acquisition of the third data point and followed by a 10 mL 0.9% NaCl flush to ensure complete delivery of the contrast medium for quantitative measurement. Phase encoding was performed left to right for all sequences.

Image Postprocessing and Analysis

Quantitative analysis of Gd-DTPA distribution was carried out using a two-compartment model, in which the concentration of Gd-DTPA is assumed to be proportional to the relative increase in FSPGR signal. Three parameters resulted from this analysis: amplitude (initial slope of signal-time curve), and the exchange and wash-out rate constants. Curve fitting of the image data on a pixel-by-pixel basis, using a simplex minimization technique (8), allowed the creation of three-color scale parameter maps for each study. A 4 × 4 mm grid was superimposed on the parameter maps using the ANALYZETM software system (Biomedical Imaging Resource, Mayo Foundation, Rochester, MN) for subsequent comparison with the histopathology specimens. As there was little or no patient movement, the same grid location was employed for each image in the dynamic series.

Histopathology

All patients underwent radical retropubic prostatectomy for presumed stage A2, B1, or B2 prostatic carcinoma within 4–6 weeks after MRI. All specimens were fixed in 5% buffered formalin for 24 hours, prior to sectioning. The entire gland was then cut by hand into 5 mm thick sections along a plane perpendicular to the posterior aspect of the prostate and each slice then halved or quartered, according to size, for further processing. Macrotome slices (7 μm thick) were obtained from the superior surface of each section and stained with hematoxylin and eosin. A total of 33 sections, which corresponded to the slice locations of the dynamic FMPSPGR sequence, were analyzed after superimposition of a transparent grid with 4 × 4 mm squares. In each case the grid was aligned as closely as possible to the orientation of the grid superimposed on the dynamic MR images. The tissue type was then recorded by location on the grid using the following classification: prostatic adenocarcinoma (poorly to well differentiated); benign prostatic hyperplasia (BPH) subdivided into glandular (with or without cystic ectasia), fibromuscular, and mixed glandular/stromal (fibroglandular); and normal stromal and glandular elements. For benign disease only squares in which a single tissue type completely filled the square were used in subsequent analysis. However, as tumors grow by infiltration, all squares containing tumor were analyzed and the percentage of tumor in each graded from 5–19%, 20–39%, 40–59%, and 60–79% to >80%.

Data Analysis

Of the 2574 grid locations examined, 1287 fulfilled the above pathological criteria. To avoid excessive partial volume averaging, only groups of at least four squares with identical benign pathology or similar grades of tumor infiltration were used for analysis. The values of the pharmacokinetic parameters for each grid location within these preselected groups were calculated and the mean value used in subsequent analysis. The data were then examined for intra-patient differences between benign and malignant tissue, using the nonparametric Wilcoxon matched-pairs signed-ranks test.

RESULTS

Of the 1287 grid locations used for analysis, 324 contained tumor, 186 fibromuscular BPH, 615 fibroglandular BPH, 36 mixed ectatic and non-ectatic glandular BPH, and 126 normal stromal and glandular elements. In three patients histology revealed only two or three squares occupied by tumor; as a result, comparison of dynamic FMPSPGR data and histology was not possible in these patients.

Only tumor and BPH in figure 1 demonstrates typical signal-intensity time curves, derived from the dynamic FSPGR data for tumor, and fibroglandular BPH, which are fitted to a two-compartment pharmacokinetic model

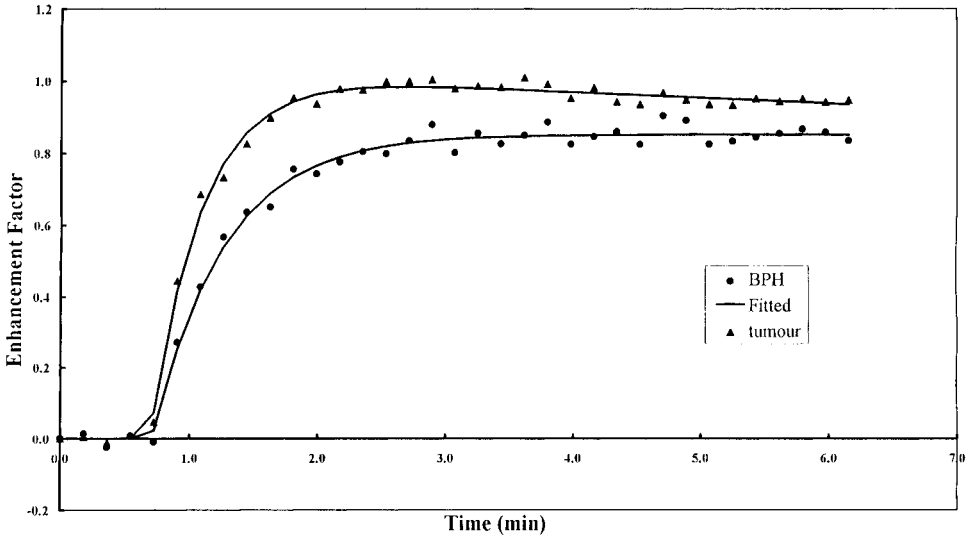

Figure 1. Typical time-signal intensity curves obtained from the FMPSPGR sequence for histologically confirmed regions of tumor and fibroglandular BPH. The enhancement factor curves generated from the FMPSPGR data for tumor and BPH demonstrate good fit with the line fitted to the data by the two-compartment pharmacokinetic model. The goodness of fit for this data is highly significant ($P < 0.001$).

for quantitative analysis. For each individual the region (group of at least four preselected grid locations) containing the greatest percentage of tumor infiltration was used in analysis. Thus regions containing 20% to 39% tumor infiltration were used in two patients, 40% to 59% in a further two patients, and >80% in five patients. The mean values obtained for the rate constant for contrast washout, amplitude of contrast washin, and rate constant for contrast exchange for the different tissue types were analyzed and are tabulated in Table 1. However, as only three patients demonstrated pure glandular BPH, analysis of this group was deemed inappropriate. Tumor demonstrated a slight increase in the amplitude of contrast uptake and the rate constant for contrast exchange compared with normal contralateral peripheral zone, but due to the small number of patients with normal peripheral zone tissue, the difference in results only approaches significance (Fig. 2).

Comparison of tumor and fibromuscular BPH revealed significantly higher values for both amplitude ($P < 0.03$) and exchange rate ($P < 0.03$) for neoplastic tissue. When tumor was compared with fibroglandular BPH, a weak difference was detected for amplitude ($P < 0.07$), but a stronger difference was obtained for the rate constant for contrast exchange ($P < 0.04$). The rate constant for contrast washout failed to differentiate any of the tissue types.

To determine the effect of the amount of tumor present on the parametric values, areas within the largest tumors containing different percentages of tumor infiltration were examined separately. In five patients calculation of the parameter values was possible for at least four of the five grades of percentage of tumor involvement determined histologically. All patients showed increasing values for both amplitude and exchange rate with increasing tumor involvement, with the exception of one patient who showed a steady increase in exchange rate from 0–19% to 60–79% tumor infiltration, but a drop at >80% infiltration (Fig. 3). No trend was apparent for the rate constant for contrast washout.

Table 1
Quantitative Analysis of Maximum Values Achieved for Washout, Amplitude and Exchange Rate for Pixels Containing Tumour, Normal Peripheral Zone Tissue and Fibromuscular and Fibroglandular BPH

	Tumour		
	Contrast washout	Amplitude of initial upslope	Contrast exchange rate
Fibromuscular BPH	z = −0.338	z = −2.201	z = −2.201
	n = 7	n = 7	n = 7
	p = 0.74	p = 0.03	p = 0.03
Fibroglandular BPH	z = −0.533	z = −1.836	z = −2.073
	n = 9	n = 9	n = 9
	p = 0.59	p = 0.07	p = 0.04
Normal peripheral zone	z = −0.730	z = −1.826	z = −1.826
	n = 4	n = 4	n = 4
	p = 0.46	p = 0.07	p = 0.07

DISCUSSION

The histological grade, location, and size of prostatic tumors are major factors in determining the ability of MRI to stage local disease accurately. Prostatic carcinoma occurs in a broad range of histological patterns that contribute to the spectrum of signal intensity changes observed. The signal intensity is dependent on the degree of cellularity and hence differentiation of the lesion, with the high cellularity and reduced fluid content of well to moderately well differentiated tumors resulting in low signal intensity (9). In contrast, poorly differentiated tumors grow by infiltration, with strands of tumor running between normal tissue causing little architectural distortion or alteration in signal intensity and making them poorly visible on MRI. Furthermore, nodules of mixed glandular and fibromuscular BPH may have a similar signal intensity to that of well-differentiated nodules of adenocarcinoma, resulting in nonvisualization of small tumors arising in the central gland or transitional zone. In addition, as tumors grow and encroach on the central gland, the margin identification is lost and the accuracy of volume estimation is reduced.

Biopsy-related changes may also account for some discrepancies in tumor delineation. Post-biopsy hemorrhage may produce either high or low signal intensity

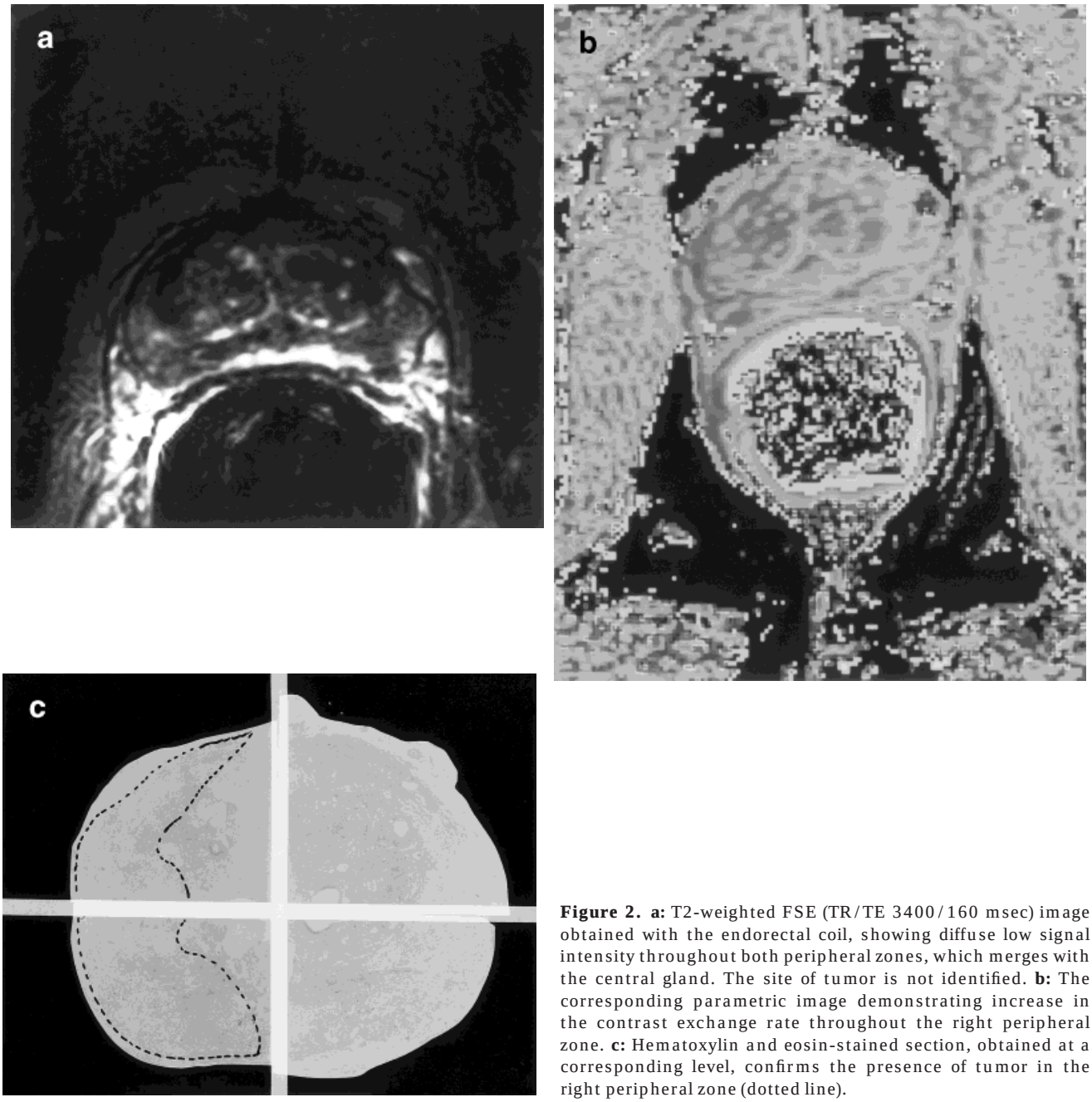

Figure 2. a: T2-weighted FSE (TR/TE 3400/160 msec) image obtained with the endorectal coil, showing diffuse low signal intensity throughout both peripheral zones, which merges with the central gland. The site of tumor is not identified. **b:** The corresponding parametric image demonstrating increase in the contrast exchange rate throughout the right peripheral zone. **c:** Hematoxylin and eosin-stained section, obtained at a corresponding level, confirms the presence of tumor in the right peripheral zone (dotted line).

artifact depending on the age of the hematoma. This may lead to overestimation of disease if the hematoma is unrecognized, or underestimation if the signal intensity changes obscure underlying capsular invasion. The prostate is also frequently the site of asymptomatic disease, namely, unsuspected chronic prostatitis, which gives rise to focal hypointensities in the peripheral zone. That these lesions may be mistaken for malignancy was demonstrated by Brem et al (10) in a study evaluating the ability of MRI to detect nonpalpable carcinoma in the contralateral lobe of patients with palpable prostatic carcinoma. Although 21 tumors were correctly identified in a study population of 53 patients, focal abnormalities were incorrectly labeled as tumor in a further 16 patients, resulting in a specificity of only 48%.

Contrast-enhanced MRI has been infrequently employed in the evaluation of prostatic cancer, and the results obtained to date are conflicting. In 1989 Kahn et al (6) examined the ability of MRI to predict tumor volume and stage preoperatively, in clinically localized prostate cancer, using T2-weighted SE and pre- and post-Gd-DTPA enhanced, T1-weighted SE images. Discrete, inhomogeneous enhancement of the prostate was demonstrated, but no enhancement of the tumor was obtained. This was contrary to a report by Nishimura et al (7), who found enhancement of the presumed tumor bearing area. In 1995, Huch Böni et al (11) used an ER coil, T2-weighted FSE, and postcontrast T1-weighted SE imaging to evaluate preoperative staging accuracy. Although Gd-DTPA-enhanced images improved the diag-

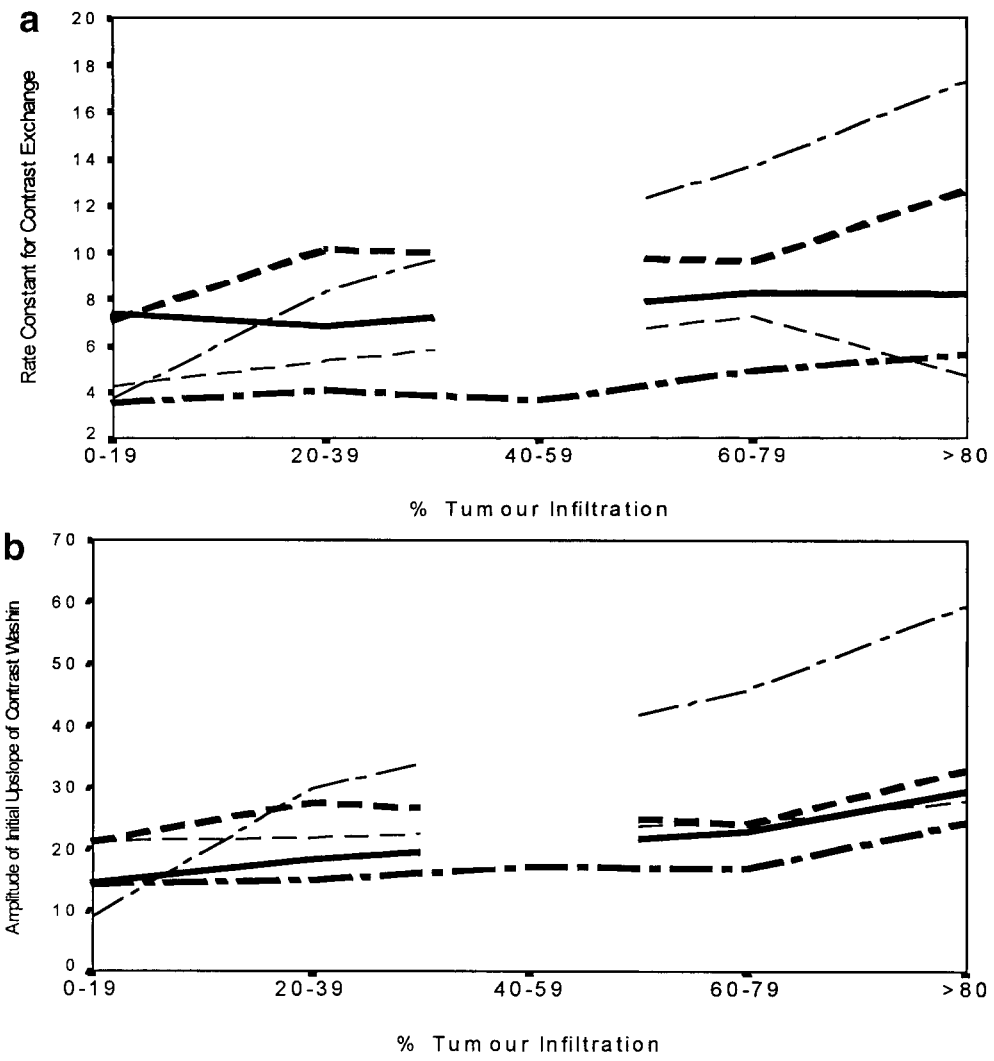

Figure 3. Effect of the amount of tumor present on the parametric values for (**a**) the rate constant of contrast exchange and (**b**) the amplitude of the initial upslope of contrast washin for five patients. Calculation of parametric values for a minimum of four of the five grades of tumor infiltration was only possible in 5 of the 12 patients.

nostic confidence of seminal vesicle and prostatic capsule involvement by 35%, it was inferior to T2-weighted FSE images for the detection of intraglandular tumor extent. Dynamic contrast enhancement has been used extensively in the investigation of other solid tumors, particularly breast disease, but has not been used to investigate prostatic pathology.

Although this study is preliminary and patient numbers small, there was a significant difference in the amplitude of the initial signal-time response curve between tumor and both fibromuscular and fibroglandular BPH and a significant difference in the rate constant for contrast exchange between tumor and fibromuscular BPH. As amplitude and exchange rate are determined by the vascularity of tissue, the differences observed may reflect the induction of new vessels by malignant tissue. The results of this study suggest that the magnitude of change observed for malignant tissue may be significantly different from that of benign disease and may allow tissue differentiation, but is influenced by the amount of tumor present, with the largest tumor loads initiating the greatest change. However, the parameter images did not provide the anatomical detail required for staging to assess the prostatic capsule, neurovascular bundles, or seminal vesicles and as such should only be used as an adjunct to conventional imaging.

There are conflicting ideas about the best method of analyzing dynamic data, but undoubtedly the accuracy with which tumors can be characterized is limited by the accuracy of estimation of the different pharmacokinetic parameters. This varies between models. In the two-compartment model used in this study, the signal maximum of tissue curves is delayed in comparison with the arterial signal, by a tissue-specific transport parameter. This characterizes the rate of exchange of Gd-DTPA between the plasma and the interstitium of the tissues. Estimation of exchange and washout rates in this model are arrived at by curve fitting; because the imaging time is relatively short, the accuracy of measurement of the washout rate is limited, which may adversely affect estimation of the exchange rate. In addition, this model, while measuring amplitude and the rate constants for contrast exchange and washout, does not take into account the preinjection T1 of the tumor, nor does it measure plasma Gd-DTPA concentration. It is possible that the accuracy of differentiating benign from malignant disease would be increased if absolute tissue parameters could be measured in vivo (12–14).

The results of this study are also influenced by inevitable errors in the location of the imaging section and the histopathological specimen slice, tissue shrinkage secondary to fixation, and partial volume averaging. In an attempt to limit these inaccuracies, analysis was restricted to clusters of four squares containing a single tissue type. This resulted in the exclusion of small tumors and BPH nodules, which would be most prone to partial volume averaging. Use of thinner histopathological sections, corresponding to a greater number of slice locations for dynamic MRI, would reduce the effect of partial volume averaging but would result in poorer temporal resolution for dynamic imaging with currently available technology. This might have detrimental effects on the ability to measure amplitude and exchange rate.

CONCLUSIONS

In summary, quantitative analysis of dynamic data using a pharmacokinetic model provided detailed analysis of the signal-time response curve on a region-by-region basis throughout the prostate. Detailed comparison with the histopathology demonstrated that the amplitude of the initial contrast uptake slope and the rate constant for contrast exchange provided good differentiation of benign from malignant disease, potentially allowing better delineation of intraglandular tumor extent compared with conventional T2-weighted FSE imaging. However, further improvement in discrimination of tumor from BPH is desirable, and various methods are currently being examined, including better spatial resolution of dynamic imaging, accurate timing of arterial enhancement, and the determination of intraglandular citrate distribution using proton MR spectroscopy and other techniques.

ACKNOWLEDGMENTS

The authors thank Drs. G. Cooksey, M. Ferro, J. Hetherington, S. Upsdell, and P. Weston, urological surgeons from the Yorkshire Region, for referring appropriate patients.

REFERENCES

1. Schnall MD, Imai Y, Tomaszewski J, Pollack HM, Lenkinski RE, Kressel HY. Prostate cancer: local staging with endorectal surface coil MRI. Radiology 1991;178:797–802.
2. Jager GJ, Barentsz JO, de la Rosette JJMCH, Rosenbusch G. Preliminary results of endorectal surface coil magnetic resonance imaging for local staging of prostate cancer. Radiologe 1994;34:129–133.
3. Chelsky MJ, Schnall MD, Seidmon EJ, Pollack HM. Use of endorectal surface coil magnetic resonance imaging for local staging of prostate cancer. J Urol 1993;150:391–395.
4. Lencioni R, Menchi D, Caramella D, Di Giulio M, Carini M, Bartolozzi C. Determining the volume of prostate carcinoma: value of MRI with an endorectal surface coil. In: Abstracts of the 12th Congress of the SMR, 1995. p1501.
5. Kaiser WA, Zeitler E. MR imaging of the breast: fast imaging sequences with and without Gd-DTPA. Radiology 1989;170:681–686.
6. Kahn T, Burrig K, Scmitz-Drager B, et al. Prostatic carcinoma and benign prostatic hypertrophy: MR imaging with histopathologic correlation. Radiology 1989;173:847–851.
7. Nishimura K, Hida S, Nishio Y, Yoshida O, Nakano Y. Clinical application of MRI for urological malignancy. 3: A new trial of MRI for bladder cancer and prostatic cancer; surface coil and Gd-DTPA. Acta Urol Jpn 1988;34:2097–3100.
8. Buckley DL, Kerslake RW, Blackband SJ, Horsman A. Quantitative analysis of multislice Gd-DTPA enhanced dynamic MR-images using an automated simplex minimization procedure. Magn Reson Med 1994;32:646–651.
9. Schiebler M, Tomaszewski J, Bezzi M, et al. Prostatic carcinoma and benign prostatic hypertrophy: correlation of high resolution MR and histopathologic findings. Radiology 1989;172:131–137.
10. Brem RF, Tempany CM, Yang A, et al. Magnetic resonance imaging in the detection of occult prostatic cancer. J Urol 1990;143:195, abstract 26.
11. Huch Böni RA, Boner JA, Lütolf UM, Trinkler F, Pestalozzi DM, Krestin GP. Contrast-enhanced endorectal coil MRI in local staging of prostatic carcinoma. J Comput Assist Tomogr 1995;19:232–237.
12. Tofts PS, Kermode AG. Measurement of the blood-brain barrier permeability and leakage space using dynamic MR imaging. 1. Fundamental concepts. Magn Reson Med 1991;17:357–367.
13. Weinmann HJ, Laniado M, Mutzel W. Pharmacokinetics of Gd-DTPA/dimeglumine after intravenous injection into healthy volunteers. Phys Chem Phys Med NMR 1984;16:167–172.
14. Hittmair K, Gomiscek G, Langenberger M, Recht K, Imhof H, Kramer J. Method for the quantitative assessment of contrast agent uptake in dynamic contrast-enhanced MRI. Magn Reson Med 1994;31:567–571.